Struct Chem (2015) 26:1287–1295
DOI 10.1007/s11224-015-0669-6

CrossMark

ORIGINAL RESEARCH

'Lanthanide contraction' in $[Ln(BTP)_3](CF_3SO_3)_3$ complexes

Attila Kovács[1] · Christos Apostolidis[1] · Olaf Walter[1] · Patric Lindqvist-Reis[2]

Received: 19 August 2015 / Accepted: 25 August 2015 / Published online: 7 September 2015

Abstract The FTIR spectra of the complexes of lanthanides (Ln = La − Lu, except for the radioactive Pm) with 2,6-bis(5,6-dipropyl-1,2,4-triazin-3-yl)pyridine have been measured in both the mid- and far-IR ranges. The spectra revealed some characteristic bands shifting towards higher wavenumbers with increasing lanthanide atomic number. X-ray diffraction results on several (La, Pr, Nd, Sm, Eu, Tm and Yb) complexes revealed decreasing Ln–ligand distances in the same direction. DFT calculations using the M062X exchange–correlation functional have been performed on selected model complexes in order to uncover the 'lanthanide contraction' phenomenon and to assist the interpretation of the FTIR spectra. The stronger bonding due to 'lanthanide contraction' is supported by the computed charge transfer interactions. The vibrational study confirmed that the blueshifting bands can be attributed to significant Ln–ligand vibrations.

Keywords 'Lanthanide contraction' · Infrared spectroscopy · X-ray diffraction · DFT · Donor–acceptor interactions

Dedicated to Professor Magdolna Hargittai on the occasion of her 70th birthday.

Electronic supplementary material The online version of this article (doi:10.1007/s11224-015-0669-6) contains supplementary material, which is available to authorized users.

✉ Attila Kovács
attila.kovacs@ec.europa.eu

[1] Institute for Transuranium Elements, European Commission, Joint Research Centre, P.O. Box 2340, 76125 Karlsruhe, Germany

[2] Institut für Nukleare Entsorgung, Karlsruhe Institute of Technology, P.O. Box 3640, 76021 Karlsruhe, Germany

Introduction

An important step in the reprocessing of spent nuclear fuel is the separation of the various components, which then are subjected to different further usages. Uranium and plutonium, used to fabricate new mixed oxide (MOX) fuels, [1] can be effectively separated by the PUREX process [2]. The radiotoxic minor actinides (Np, Am, Cm) possessing long decay should be transmuted to short-lived radionuclides by neutron bombardment [3]. The efficiency of this process, however, is hindered by the lanthanide components, which have large neutron absorption cross sections and therefore have to be removed selectively.

The trivalent lanthanide ions have very similar chemical properties to the trivalent americium and curium ions. Their separation is based on a liquid–liquid extraction process using complexing ligands with soft donor atoms, which are likely to bind stronger to the actinides than to the lanthanides owing to the somewhat stronger donor–acceptor abilities of the actinide 5*f* and 6*d* atomic orbitals with the molecular orbitals of the soft donor ligands than the 4*f* orbitals of the lanthanides. The key element in these ligands is the soft donor nitrogen atom in an aromatic environment. From the large number of heterocyclic N-donor extractants tested [4], 2,6-bis([1,2,4]-triazin-3-yl)pyridines (BTPs) proved to be a most effective and convenient option [5]. The main factor for the efficient binding of trivalent actinides likely lies in the smaller steric demands of the [1,2,4]-triazin-3-yl ring with respect to the 2-pyridinyl ring, allowing the nitrogens to approach more closely to the metal. Another advantage of BTPs as extraction ligands is that they work also in highly acidic aqueous solutions, generally used in the reprocessing of spent fuel.

The focus in this research field has been to elucidate the differences between actinides and lanthanides [5–11] upon

binding to BTP ligands, while less attention was paid to the characteristics within the Ln series. It can be expected that if the 'lanthanide contraction' [12, 13] is significant in these complexes, the metal–ligand interactions should increase along the Ln series. Indeed, the Ln elements have been found to show a trend in selectivity as a function of their ionic radii [14]. Hence, the two goals of our present study were (1) to elucidate the contraction effects in $[Ln(BTP)_3]$ complexes and (2) to determine the character and trend of the interactions. This has been achieved by a joint application of experimental (FTIR, Raman and X-ray) and theoretical (DFT calculations) methods.

Experimental

General preparation procedure of the complexes $[Ln(BTP)_3](CF_3SO_3)_3$

Approximately 45 mg (~0.13 mmol) of $[Ln(H_2O)_9](CF_3SO_3)_3$ was dissolved in 1 ml EtOH, and then three equivalents of 2,6-bis(5,6-dipropyl-1,2,4-triazin-3-yl)pyridine (~65 mg) in 1 ml EtOH (dissolved at elevated temperature) were added. On slow cooling to room temperature, the complexes form crystals of the constitution $[Ln(BTP)_3](CF_3SO_3)_3$*EtOH in yields of 50–60 %. By further evaporation of the solvent, more complex precipitated resulting in an overall yield above 95 %. The MeCN adduct of Pr was formed by re-crystallisation of the obtained precipitate in MeCN.

IR spectroscopy

IR spectroscopic measurements were taken on a Perkin Elmer Spectrum 1000 FT spectrometer on KBr pellets for the MIR range (4000–400 cm^{-1}) and polyethylene pellets for the FIR range (400–120 cm^{-1}) with a resolution of 2 cm^{-1}.

Raman spectroscopy

The Raman spectra of $[Ln(BTP)_3](CF_3SO_3)_3$ (Ln = La, Sm, Eu and Gd) were measured at room temperature using a Bruker Senterra dispersive Raman microscope at 785 nm, 25 mW, at a spectral resolution of 4 cm^{-1}. For each compound, eight spectra were averaged and background was corrected using the OPUS software from Bruker.

Crystallographic data

The XRD measurements were taken on a Siemens SMART CCD 1000 diffractometer [15] with monochromated MoKα radiation collecting a full sphere of data (La, Eu) or a Bruker Apex II Quazar diffractometer [16] collecting four full spheres of data (Pr, Nd). Frames were collected with an irradiation time of 20 or 10 s per frame and ω-scan technique with $\Delta\omega = 0.45°$ on the SMART diffractometer, whereas on the Apex II diffractometer a mixed ω- and φ-scan technique was employed for data collection with $\Delta\omega = \Delta\varphi = 0.5°$ with irradiation times of 12 s per frame appropriate to size and diffracting abilities of the crystals. Data were integrated with SAINT, corrected to Lorentz and polarisation effects, and an empirical adsorption correction with SADABS was applied. The structures were solved by direct methods and refined to an optimum $R1$ value with SHELX-2013 [17]. Visualisation for evaluation was performed with xpma [18], and the figures were created with Winray-32 [19]. For more detailed explanations, see Table 1.

The structures have been deposited at the Cambridge Crystallographic Data Centre with the reference CCDC numbers 1405122-1405125, and they contain the supplementary crystallographic data for this paper. These data can be obtained free of charge from the CCDC via www.ccdc.cam.ac.uk/data_request/cif.

Computational details

The large size of the BTP ligand necessitated to a truncation in the model structures. The *n*-propyl chains are expected to exert a very small influence on the electronic interactions between Ln and BTP, and therefore, in the calculation of the Ln series, they were replaced by hydrogens. The truncated ligand is denoted in the following as BTP′. The applicability of BTP′ was confirmed by a test calculations on the La complexes: the La–N distances comparing $La(BTP)_3$ and $La(BTP')_3$ were within 0.01 Å. (The Cartesian coordinates of the computed $[La(BTP')_3]$ and $[La(BTP)_3](CF_3SO_3)_3$ structures are given as Supplementary Material.)

In contrast, the aliphatic groups are needed for proper modelling of the experimental IR spectra. As the calculation of vibrational frequencies failed for the complex with the *n*-propyl groups, they were replaced by ethyl groups. This truncation caused changes by a few thousandths of angstrom in the La–N distances.

The computations were performed with the Gaussian 09 suit of programs [20] using the M062X [21] exchange–correlation functional in conjunction with the Stuttgart–Cologne 4*f*-in-core quasi-relativistic pseudopotentials for the lanthanides [22, 23]. The valence basis set treating the 5*s*5*p*5*d*6*s* orbitals had the contraction scheme of [7*s*6*p*5*d*]/[5*s*4*p*3*d*] [22]. For N, C and H, the standard 6-31G** basis set was used. Test calculations using the more expensive small-core 4*f*-in-valence quasi-relativistic pseudopotentials [24] were performed on the Ce and Tm complexes. The valence

Table 1 Crystallographic details of the measured $[Ln(BTP)_3](CF_3SO_3)_3$ ([Ln]) complexes

Compound	[La]*EtOH	[Pr]*2.4 MeCN	[Nd]*EtOH	[Eu]*EtOH
Formula	$C_{74}H_{102}F_9N_{21}LaO_{10}S_3$	$C_{76.8}H_{100}F_9N_{23}PrO_9S_3$	$C_{74}H_{102}F_9N_{21}NdO_{10}S_3$	$C_{74}H_{102}F_9N_{21}EuO_{10}S_3$
Formula weight	1848.83	1903.29	1857.18	1864.88
Temperature	200(2) K	100(2) K	100(2) K	200(2) K
Wavelength	0.71073 Å	0.71073 Å	0.71073 Å	0.71073 Å
Crystal system	Triclinic	Triclinic	Triclinic	Triclinic
Space group	$P\bar{1}$	$P\bar{1}$	$P\bar{1}$	$P\bar{1}$
Unit cell dimensions				
a	13.267(5) Å	13.3040(8) Å	13.252(1) Å	13.2923(9) Å
α	91.793(7)°	97.203(1)°	91.746(1)°	91.735(1)°
b	b = 13.288(6) Å	b = 15.7360(9) Å	b = 13.250(1) Å	b = 13.3829(9) Å
β	101.677(7)°	93.450(1)°	101.985(1)°	101.987(1)°
c	26.016(11) Å	22.020(1) Å	26.025(2) Å	26.185(2) Å
γ	110.165(7)°	100.228(1)°	110.186(1)°	110.276(1)°
Volume	4191(3) $Å^3$	4484.7(5) $Å^3$	4169.5(6) $Å^3$	4247.5(5) $Å^3$
Z	2	2	2	2
Density (calc.)	1.465 Mg m^{-3}	1.409 Mg m^{-3}	1.479 Mg m^{-3}	1.456 Mg m^{-3}
Abs. coefficient	0.673 mm^{-1}	0.698 mm^{-1}	0.787 mm^{-1}	0.900 mm^{-1}
$F(000)$	1912	1970	1924	1784
Crystal size (mm^3)	0.15 × 0.3 × 0.3	0.059 × 0.0141 × 0.194	0.09 × 0.04 × 0.02	0.15 × 0.25 × 0.35
θ range	1.608°–28.591°	0.935°–28.546°	1.610°–28.283°	1.600°–28.294°
Index ranges	$-17 \le h \le 17$,	$-17 \le h \le 17$,	$-17 \le h \le 17$,	$-17 \le h \le 17$,
	$-17 \le k \le 17$,	$-20 \le k \le 20$,	$-17 \le k \le 16$,	$-17 \le k \le 17$,
	$-34 \le l \le 34$	$-29 \le l \le 29$	$-34 \le l \le 34$	$-34 \le l \le 34$
Reflections				
Collected	57,758	82,088	74,828	51,731
Independent	20,383	20,757	19,060	20,385
	[R(int) = 0.1631]	[R(int) = 0.0568]	[R(int) = 0.0753]	[R(int) = 0.0508]
Observed [$I > 2\sigma(I)$]	10,019	16,712	13,987	16,156
Coverage (θ = 25°)	99.8 %	99.6 %	99.6 %	99.8 %
Data/restraints/parameters	20,383/102/1145	20,757/220/1245	19,060/0/1091	20,385/60/1145
Goof on F^2	1.064	1.024	1.025	1.027
R indices [$I > 2\sigma(I)$]	$R1$ = 0.1200	$R1$ = 0.0487	$R1$ = 0.0521	$R1$ = 0.0502
R indices (all data)	$wR2$ = 0.2990	$wR2$ = 0.1269	$wR2$ = 0.1140	$wR2$ = 0.1139
Largest peak/hole	2.150/−3.685 e $Å^{-3}$	1.185/−1.303 e $Å^{-3}$	1.461/−1.609 e $Å^{-3}$	1.013/−0.944 e $Å^{-3}$

basis set treating the 4*s*4*p*4*d*4*f*5*s*5*p*5*d*6*s* orbitals had the contraction scheme of [14*s*13*p*10*d*8*f*6*g*]/[10*s*8*p*5*d*4*f*3*g*] [25]. These results agree with the main features of 'lanthanide contraction' predicted by the 4*f*-in-core calculations. The atomic charges and charge transfer properties were assessed using the natural bond orbital (NBO) model [26] by means of the NBO 5.9 code [27].

Results and discussion

The Ln(III) and An(III) ions form 1:3 complexes with charge–neutral BTP-type ligands, in which BTP acts as a tridentate ligand [8, 28] (Fig. 1). The metal is bonded to the pyridine (N_1) and two azine nitrogens (N_2, $N_{2'}$). In the complex molecule, the three BTP ligands surround the metal ion in a spherical fashion with dihedral angles of around 120°/240° between the planes of the ligands. As BTP is neutral, the $[Ln(BTP)_3]$ moieties have a charge of +3 from the Ln(III) ion. Trifluoromethanesulfonate, $CF_3SO_3^-$, was used as counter ion both in the experiments and modelling of the IR spectra. This structure from the computations is presented in Fig. 2.

The main structural features of the complex molecules in the crystal agree with those of the isolated molecules from the computations. The coordination sphere around the lanthanide ion is ninefold (Fig. 3). Three N atoms of each BTP ligand are embedded in coordinative bonds. The nine

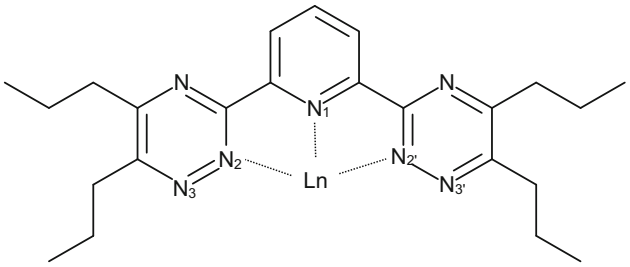

Fig. 1 Coordination of lanthanides and actinides to BTP

donor N atoms form a distorted tri-capped prismatic arrangement around the metal ion with more or less equal Ln–N distances in the range of 2.45–2.65 Å (see Table 2) exhibiting no real differences between the Ln–N bond distances to a pyridine or a triazine unit. With these findings, the described structural features of the $[Ln(BTP)_3]^{3+}$ complex cations are in good agreement with literature reports on BTP [28], BTP derivative complexes [7, 29, 30] or complexes with comparable structural motifs arising from ligands which are related to BTP in terms of symmetry and coordination behaviour [5, 31–42].

The experimentally determined structures of the crystalline $[La(BTP)_3](CF_3SO_3)_3$*EtOH, $[Nd(BTP)_3](CF_3SO_3)_3$*EtOH, $[Eu(BTP)_3](CF_3SO_3)_3$*EtOH compounds are virtually identical due to isostructural crystal formation (cf. Table 1). The Pr complex, however, does not crystallize well from the solvent of choice (EtOH). Using MeCN as solvent, crystals with the

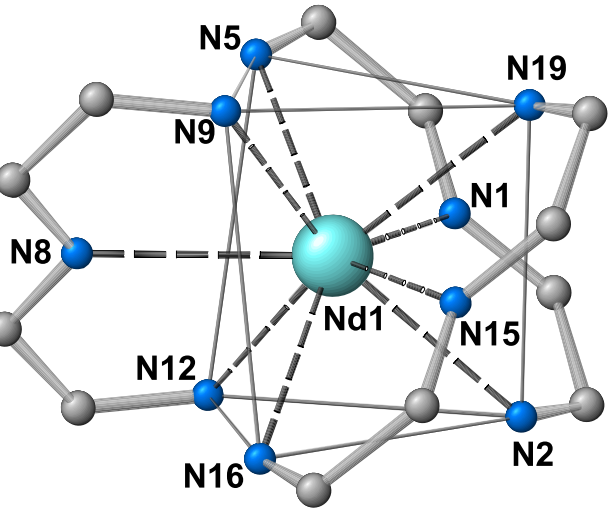

Fig. 3 Ninefold coordination sphere around the lanthanide ion. The numbering of atoms corresponds to those in the cif (X-ray structure) files

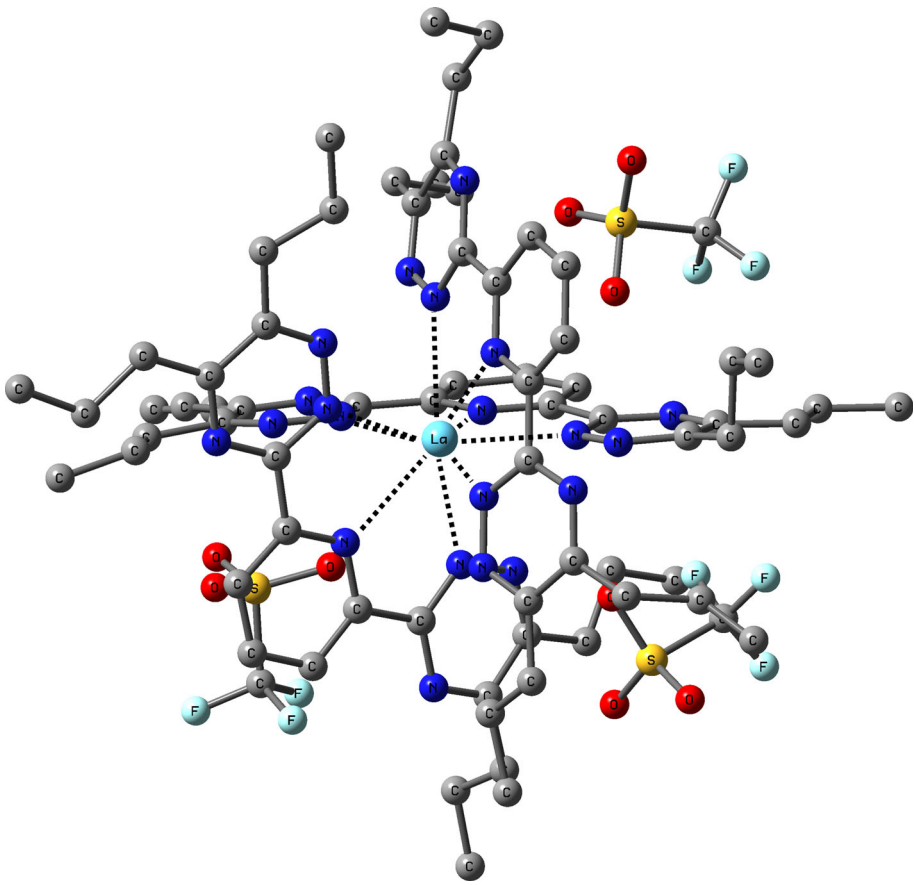

Fig. 2 Structure of the computed $[La(BTP)_3](CF_3SO_3)_3$ complex (hydrogens are not depicted)

Table 2 Selected bond distances (Å) from X-ray diffraction on $[Ln(BTP)_3](CF_3SO_3)_3$ and computations on $[Ln(BTP')_3]$ complexes

Ln	Calculated					X-ray[a]	
	$Ln–N_1$	$Ln–N_2$	$N_1–C$	$N_2–N_3$	$N_2–C$	$Ln–N_1$	$Ln–N_2$
La	2.698	2.673	1.342	1.328	1.333	2.611(9)	2.585(9)
Ce	2.673	2.652	1.342	1.328	1.333		
Pr	2.652	2.638	1.341	1.328	1.333	2.600(3)	2.596(3)
Nd	2.632	2.622	1.341	1.328	1.333	2.598(3)	2.584(3)
Pm	2.618	2.610	1.341	1.328	1.333		
Sm	2.602	2.599	1.340	1.328	1.333	2.574(9)	2.572(9)
Eu	2.588	2.587	1.340	1.328	1.334	2.556(3)	2.557(3)
Gd	2.576	2.577	1.340	1.328	1.334		
Tb	2.564	2.565	1.340	1.327	1.334		
Dy	2.553	2.558	1.340	1.327	1.334		
Ho	2.543	2.550	1.339	1.327	1.334		
Er	2.532	2.539	1.339	1.327	1.334		
Tm	2.522	2.531	1.339	1.327	1.334	2.486(7)	2.505(7)
Yb	2.513	2.522	1.339	1.327	1.334	2.460(9)	2.475(9)
Lu	2.502	2.515	1.339	1.327	1.334		
BTP′			1.337	1.330	1.344		

[a] The X-ray data are the average values of the slightly asymmetric experimental results. The data of the Sm, Tm and Yb complexes were taken from Ref. [28]

composition of $[Pr(BTP)_3](CF_3SO_3)_3$*2.4 MeCN were obtained. Differences in crystal packing between the two families of compounds with ethanol or acetonitrile adducts influenced very slightly the Ln–O distances (vide infra).

Selected geometrical parameters from our (La, Pr, Nd, Eu) and literature (Sm, Tm, Yb) [28] X-ray studies and from our computations are compared in Table 2. The experimental and calculated bond distances are in good agreement (taking into account the approximations used in our modelling, the intermolecular effects in the solid state, and the different physical meaning of the distance parameter from the two methods [43]). Most interesting are the $Ln–N_1$ and $Ln–N_2$ distances representing the bonding between the lanthanide and BTP(BTP′) ligands. These distances are between 2.4 and 2.7 Å, and around the sums of the ionic and covalent radii of Ln and N (e.g. the sum of covalent radii of La and N is 2.78 Å [44]; the sum of ionic radii is 2.62 Å [45]). This is in agreement with the mixed ionic/covalent character of the bonding in such complexes. The $Ln–N_3$ distance is around 3.5 Å indicating very weak interaction in the van der Waals range. We note that while the computations resulted in a symmetric Ln–BTP′ arrangement, in the crystal the packing introduces minor deviations: within an $Ln(BTP)_3$ moiety, both the $Ln–N_1$ and $Ln–N_2$ distances can differ up to 0.03 Å. For an easier comparison, in Table 2 we presented the average values.

The main question in the discussion of the geometry is the ‘lanthanide contraction’ [12, 13]. This can be well recognised in both the experimental and computed Ln–N distances. The decreasing trend (ca. 0.2 Å from La to Lu) is nearly parallel to the Ln^{3+} ionic radii (cf. Figure 4).

The bonds within the BTP′ ligand are considerably less affected. As the computed data in Table 2 show, the $N_1–C$ bond shows a slight sensitivity on the atomic number of the lanthanide (0.003 Å from La to Lu), while the effect in $N_2–N_3$ and $N_2–C$ is negligible. As these changes are within experimental error, they cannot be observed in the X-ray data. Comparing some characteristic geometrical parameters of BTP′ in the complexes with those of the free ligand (cf. Table 2), we can observe a lengthening of $N_1–C$, while shortenings of $N_2–N_3$ and $N_2–C$ in the complex. These changes are associated with the change in the electron density distribution in the ligand upon complex formation.

Very interesting is the relative magnitude of the $La–N_1$ and $La–N_2$ distance demonstrated by the data in Table 2 and Fig. 4. At the beginning of the lanthanide row, $La–N_1 > La–N_2$ ($\Delta = 0.025$ Å), which turns over from the middle of the row to $Lu–N_1 < Lu–N_2$ ($\Delta r = 0.015$ Å). The trend can also be recognised in the available experimental data. We note that the slightly deviating experimental $Pr–N_2$ distance can be explained by the somewhat different cell structure of this compound compared with the other measured complexes (vide supra). The trend points to a significant change in the Ln…BTP′ interactions as the atomic number of Ln increases.

The origin of the presented feature lies in the ‘lanthanide contraction’. As shown in Fig. 4, the $Ln–N_1$ distance

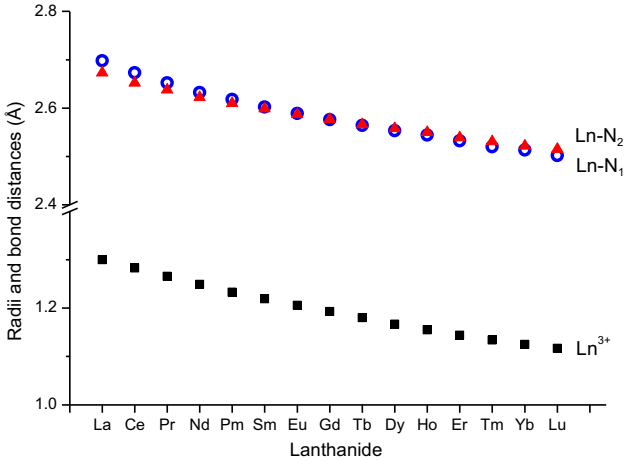

Fig. 4 Computed Ln–N bond distances and the Ln^{3+} ionic radii. N_1 and N_2 correspond to the pyridine and azine nitrogens, respectively (cf. Figure 1)

changes parallel with the Ln^{3+} ionic radii. It indicates that the approach of the pyridine nitrogen by the Ln ion is controlled by the Ln^{3+} radius. At the same time, the less flexible azine nitrogens cannot accommodate in the same degree to the decreasing Ln–N_1 distance; hence, the decrease in the Ln–N_2 distance is somewhat less pronounced. In this way, the different behaviour of the two Ln–N distances can qualitatively be explained by steric reasons.

In order to uncover the consequences of this effect on the bonding interactions in the complexes, we investigated the atomic charges and charge transfer interactions by means of the NBO method [26].

The computed bonding data of the La and Lu complexes are compared in Table 3. The natural charges are around 2 e, indicating a strong ionic character of the Ln–BTP′ interaction. From the two binding nitrogens, N_1 has a larger negative character in the complexes and hence a stronger ionic interaction with Ln.

The main covalent contributions consist of donations from the lone pairs (LP) of N_1 and N_2 to the empty valence orbitals of Ln and from the backdonation from Ln to the π^* antibonding orbitals of the N_1–C, N_2–N_3 and N_2–C bonds (cf. Table 3). In agreement with the stronger electrostatic interaction of Ln with N_1, the donation from the LP of this nitrogen is smaller than the donation from the LP of N_2. In contrast, the back donation to the pyridine and triazine rings is similar in terms of energy.

Along the lanthanide row, the following trends can be recognised in Table 3: (1) The atomic charge of the lanthanide decreases from La to Lu, while no change can be observed in the natural charges of N_1 and N_2 (the compensating charge increase is dissipated in the inner part of the ligand). These observations point to somewhat

Table 3 Comparison of charge transfer properties[a] in $[La(BTP')_3]$ and $[Lu(BTP')_3]$ from NBO analysis

Property	La	Lu
n(Ln)	+2.14	+2.04
$n(N_1)$	−0.56	−0.56
$n(N_2)$	−0.38	−0.38
$N_1(LP) \rightarrow Ln$	80	164
$N_2(LP) \rightarrow Ln$	162	185
$Ln \rightarrow N_1–C(\pi^*)$	87	123
$Ln \rightarrow N_2–N_3(\pi^*)$	32	46
$Ln \rightarrow N_2–C(\pi^*)$	55	74

[a] Natural charge, *n* (e), second-order perturbation energies (kJ mol^{-1}). The data including N_3 refer to one triazine ring

weakening ionic interactions from La to Lu. (2) All charge transfer energies are significantly increased in the Lu complex as compared to $[La(BTP')_3]$ meaning the increase in covalent interactions. (3) The charge transfer interactions between Ln and N_1 are considerably more evident in $[Lu(BTP')_3]$ than the charge transfer interactions between Ln and N_2. This is in agreement with the more pronounced shortening of the Ln–N_1 bond distances from La to Lu than that of the Ln–N_2 bond lengths, resulting in a turnover in the relative magnitudes (vide supra).

The experimental FTIR spectra of the $[Ln(BTP)_3](CF_3SO_3)_3$ series show slight differences with the change of the lanthanide from La to Lu. (The list of the band positions and intensities is available as Table S1 in the Supplementary Material.) In order to interpret these changes properly, we had to assign the absorption bands in the spectra first, which was done with the help of the calculations. The calculated IR spectrum of the La complex is compared with the experimental one in Fig. 5. In the figure, the calculated frequencies above 1100 cm^{-1} are scaled by a factor of 0.940, suggested for the M06-2X/6-31+G** level (differing only by a set of diffuse functions from our basis set) [46].

The two spectra in Fig. 5 are in good agreement, confirming that our calculations can provide a proper interpretation of the experimental IR spectrum. This has been performed by qualitative visual observation of the fundamentals by means of the GaussView program [47], facilitating the recognition of their main vibrational components. The bands of the $CF_3SO_3^-$ counter ions were supported by literature IR data on rare earth trifluoromethanesulfonate crystals [48]. The characterisation of selected important peaks of $[La(BTP)_3](CF_3SO_3)_3$ is given in Table 4.

In Fig. 6a, we show the range of 400–600 cm^{-1} of the experimental IR spectra, which demonstrates nicely the

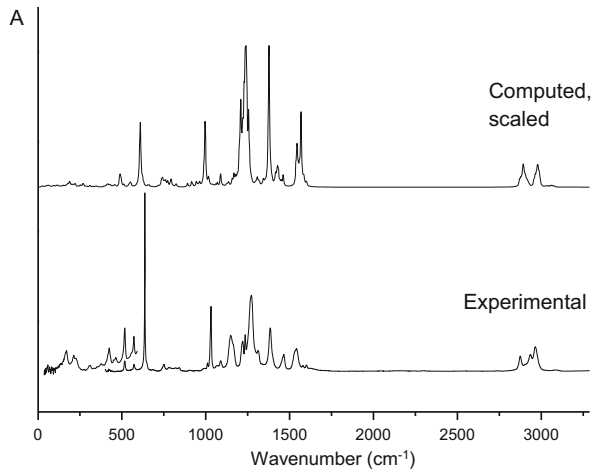

Fig. 5 Comparison of the experimental and computed (scaled) IR spectra of $[La(BTP)_3](CF_3SO_3)_3$

modifications induced by exchanging of the lanthanide. The bands at 423 and 463 cm^{-1} in the spectrum of the La complex show a significant gradual shift up to 433 and 470 cm^{-1}, respectively, in the spectrum of the Lu complex. A qualitative agreement with the trend of Ln^{3+} ionic radii and calculated Ln–N bond distances, shown in Fig. 4, can be well recognised. Hence, the experimental IR data confirm the appearance of 'lanthanide contraction' in $[Ln(BTP)_3](CF_3SO_3)_3$ complexes.

The fundamentals affected by the 'lanthanide contraction' are complex, but all contain some movement of the Ln atom. In the high-wavenumber fundamentals, these correspond to Ln–N stretching vibrations, while in the low-wavenumber region bending, mainly out-of-plane bending (with respect to the plane of the aromatic ring) vibrations.

The experimental wavenumbers of the most characteristic blueshifting bands are compiled in Fig. 6b involving all the studied lanthanides. The magnitude of shifts from La to Lu amounts to 7–10 cm^{-1}. There are two somewhat different behaviours in the depicted trends: for ν_1–ν_3 and ν_6 the changes in the band positions are monotonic from La to Lu, while for ν_4 and ν_5 the majority of the shift appears in the first lanthanides (La–Nd), and the change in the second part of the Ln row is considerably smaller. This can probably be attributed to a change in the composition of these latter normal modes, probably to a decreasing Ln–N contribution. However, the change in this contribution is so small that it cannot be recognised by a qualitative visualisation.

In contrast to IR, the room temperature Raman spectra of solid $[Ln(BTP)_3](CF_3SO_3)_3$ (Ln = La, Sm, Eu, Gd) complexes given in the Supplementary Material as Figure S1 and Table S2 show no obvious shifts of any characteristic band.

Conclusions

Lanthanide complexes with 2,6-bis(5,6-dipropyl-1,2,4-triazin-3-yl)pyridine show clearly the effects of 'lanthanide contraction'. Evidences of the Ln–N bond contraction appear both in the X-ray data and in the shift of some bands in the FTIR spectra.

We performed DFT calculations on model structures in order to uncover the bonding basis of the contraction effects in these complexes and to assist the interpretation of the experimental IR spectra. The computed geometries revealed that upon contraction the covalent interactions of Ln with the pyridine ring strengthen somewhat more than

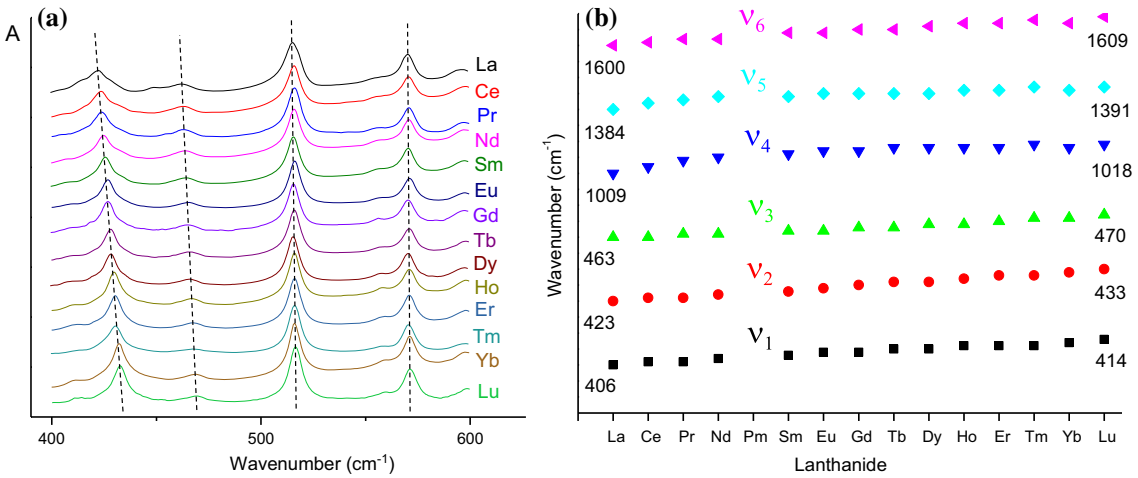

Fig. 6 **a** The 400–600 cm^{-1} section of the FTIR spectra of $[Ln(BTP)_3](CF_3SO_3)_3$ complexes demonstrating the effect of 'lanthanide contraction' on the vibrational frequencies. **b** Selected experimental fundamental frequencies

Table 4 Assignment of the characteristic bands in the IR spectra of $[La(BTP)_3](CF_3SO_3)_3$ on the basis of M06-2X/6-31G** calculations

Experimental	Computed[a]	Main character[b]
167, w	158, w	$\beta(Aza–C_{CH2})$
210, w	197, w	$\tau(CH_3)$
224, sh	231, w	$\gamma(Aza–Py)$
273, w	281, w	$\tau(CH_3)$
308, w	305, w	$\tau(Aza)$
332, w	323, w	$\beta(Aza–Py)$
348, w	343, w	$\beta(C_{Aza}–C_{CH2}–C_{CH3})$
406, sh	413, w	$\tau(Aza,Py)$
423, m	439, m	$\tau(Aza,Py)$
463, w	482, w	$\tau(Aza)$
517, m	523, w	$\delta_{as}(SO_3,CF_3)$
572, w	579, w	$\delta_{as}(SO_3,CF_3)$
636, s	645, s	$\delta_{s}(SO_3,CF_3)$
648, sh	651, w	$\beta(Aza)$
750, w	779, w	$\delta(CH_3)$, $\delta(CH_2)$, $\gamma(CH)_{Py}$
782, w	805, w	$\tau(Aza)$
821, w	840, w	$\delta(CH_3)$, $\delta(CH_2)$, $\gamma(CH)_{Py}$)
842, w	874, w	$\gamma(CH)_{Py}$
1009, w	1020, w	$\beta(Aza)$, $\nu(CC)_{propyl}$
1031, s	1057, s	$\nu_s(SO_3)$
1089, m	1153 (1084), w	$\nu(C_{Aza}–CH_2)$
1149, m	1200 (1128), w[c]	$\nu(Aza)$, $\gamma(CH_2)$
1221, m	1274 (1198), w	$\nu_{as}(CF_3)$
1235, m	1282 (1205), s	$tw(CH_2)$
1272, s	1316 (1237), s	$\nu(CS)$, $\nu_{as}(SO_3)$, $\nu_{as}(CF_3)$
1312, m	1333 (1253), m	$\gamma(CH_2)$
1384, s	1462 (1374), s	$\beta(CH_2)$, $\nu(Aza)$, $\nu(Py)$
1465, m	1517 (1425), m	$\delta_{as}(CH_3)$
1533, sh	1639 (1541), s	$\nu(Aza)$ with strong $\nu(CC)$
1540, m	1665 (1565), s	$\nu(Aza)$ with strong $\nu(CN)$, $\nu(NN)$
1579, w	1685 (1584), w	$\nu(Py)$ with strong $\nu(CN)$
1600, w	1701 (1599), w	$\nu(Py)$, $\nu(Aza)$ with strong $\nu(CN)$
2875, m	3054 (2870), m	$\nu_s(CH_2)$
2907, sh	3078 (2893), s	$\nu_s(CH_3)$
2936, m	3141 (2952), m	$\nu_{as}(CH_2)$
2965, s	3171 (2981), s	$\nu_{as}(CH_3)$
3081, wbr	3221 (3028), m	$\nu(CH_{Py})$

[a] Harmonic frequencies. The values in parentheses above 1100 cm^{-1} were obtained by a uniform scale factor of 0.940 [46]. Qualitative computed IR intensity is given, as several close-lying fundamentals superimpose in the computed spectrum

[b] The meaning of vibrational symbols is the following: ν, stretch; β, bend; δ, deformation, γ, out-of-plane bend; tw, twist, τ, torsion. The notations mean: s, symmetric; as, asymmetric, Py, pyridine; Aza, triazine

[c] The eye-catching discrepancy between the experimental and computed intensity is likely due to the truncation of the BTP propyl groups in the frequency calculation. The respective band appears in both the experimental and computed IR spectrum of the free BTP ligand with considerably intensity

with the triazine ring. This is due to the more pronounced increasing charge transfer interactions between Ln and N_1 compared to those with N_2. Hence, the specialities of the 'lanthanide contraction' are related to these different covalent interactions with the pyridine and triazine rings.

Analysis of the fundamental vibrations revealed that the blueshifting bands are attributed to modes including significant metal–ligand vibrations, particularly in which the Ln-N distance changes or Ln moves out of the ligand plane.

Supplementary Material

The online version of this article contains supplementary material (list of experimental IR and Raman data, Cartesian coordinates of the computed $[La(BTP')_3]$ and $[La(BTP)_3](CF_3SO_3)_3$ structures are given), which is available to authorised users.

References

1. Durret LF, Capus G (1998) Rev Génér Nucl 4:38
2. Choppin G, Liljenzin J-O, Rydberg J (2002) Radiochemistry and nuclear chemistry. Butterworth-Heinemann, Woburn
3. Madic C, Hudson MJ, Liljenzin JO, Glatz JP, Nannicini R, Facchini A, Kolarik Z, Odoj R (2002) Prog Nucl Energy 40:523
4. Geist A, Hill C, Modolo G, Foreman MRSJ, Weigl M, Gompper K, Hudson MJ (2006) Solv Extr Ion Exch 24:463
5. Berthet JC, Miquel Y, Iveson PB, Nierlich M, Thuery P, Madic C, Ephritikhine M (2002) J Chem Soc Dalton Trans 3265
6. Panak PJ, Geist A (2013) Chem Rev 113:1199
7. Iveson PB, Rivière C, Guillaneux D, Niederlich M, Thuéry P, Epheritikine M, Madic C (2001) Chem Commun 1512
8. Denecke MA, Rossberg A, Panak PJ, Weigl M, Schimmelpfennig B, Geist A (2005) Inorg Chem 44:8418
9. Maldivi P, Petit L, Adamo C, Vetere V (2007) C R Chim 10:888
10. Banik NL, Schimmelpfennig B, Marquard CM, Brendebach B, Geist A, Denecke MA (2010) Dalton Trans 39:5117
11. Dupont C, Hill C, Suzenet F, Guillaumet G (2013) Solv Extr Ion Exch 31:253
12. Hargittai M (1988) Coord Chem Rev 91:35
13. Hargittai M (2000) Chem Rev 100:2233
14. Steppert M, Walther C, Geist A, Fanghänel T (2009) New J Chem 33:2437
15. SMART, SAINT, SADABS, Siemens (1997) Analytical X-ray instruments Inc. Karlsruhe, Germany
16. APEX2, SAINT-Plus, SADABS (2007) Bruker AXS Inc., Madison, Wisconsin, USA
17. Sheldrick GM (2008) Acta Cryst A64:112

18. Zsolnai L, Huttner G (1994) XPMA, University of Heidelberg
19. Soltek R, Huttner G (1998) winray-32, University of Heidelberg
20. Frisch MJ, Trucks GW, Schlegel HB, Scuseria GE, Robb MA, Cheeseman JR, Scalmani G, Barone V, Mennucci B, Petersson GA, Nakatsuji H, Caricato M, Li X, Hratchian HP, Izmaylov AF, Bloino J, Zheng G, Sonnenberg JL, Hada M, Ehara M, Toyota K, Fukuda R, Hasegawa J, Ishida M, Nakajima T, Honda Y, Kitao O, Nakai H, Vreven T, Montgomery JA Jr, Peralta JE, Ogliaro F, Bearpark M, Heyd JJ, Brothers E, Kudin KN, Staroverov VN, Kobayashi R, Normand J, Raghavachari K, Rendell A, Burant JC, Iyengar SS, Tomasi J, Cossi M, Rega N, Millam MJ, Klene M, Knox JE, Cross JB, Bakken V, Adamo C, Jaramillo J, Gomperts R, Stratmann RE, Yazyev O, Austin AJ, Cammi R, Pomelli C, Ochterski JW, Martin RL, Morokuma K, Zakrzewski VG, Voth GA, Salvador P, Dannenberg JJ, Dapprich S, Daniels AD, Farkas Ö, Foresman JB, Ortiz JV, Cioslowski J, Fox DJ (2009) Gaussian 09, Revision C.01, Gaussian, Inc., Wallingford, CT
21. Zhao Y, Truhlar DG (2008) Theor Chem Acc 120:215
22. Dolg M, Stoll H, Savin A, Preuss H (1989) Theor Chim Acta 75:173
23. Dolg M, Stoll H, Preuss H (1993) Theor Chim Acta 85:441
24. Dolg M, Stoll H, Preuss H (1989) J Chem Phys 90:1730
25. Cao X, Dolg M (2002) J Mol Struct (Theochem) 581:139
26. Reed AE, Curtiss LA, Weinhold F (1988) Chem Rev 88:899
27. Glendening ED, Badenhoop JK, Reed AE, Carpenter JE, Bohmann JA, Morales CM, Weinhold F (2011) NBO 5.9, Theoretical Chemistry Institute, University of Wisconsin, Madison, US
28. Drew MGB, Guillaneux D, Hudson MJ, Iveson PB, Russell ML, Madic C (2001) Inorg Chem Commun 4:12
29. Fedosseev AM, Grigoriev MS, Charushnikova IA, Budantseva NA, Starikova ZA, Moisy P (2008) Polyhedron 27:2007
30. Guillet GL, Hyatt IFD, Hillesheim PC, Abboud KA, Scott MJ (2013) New J Chem 37:119
31. Frost GH, Hart FA, Heath C, Hursthouse MB (1969) J Chem Soc D 1421
32. Piquet C, Williams AF, Bernardinelli G, Bunzli J-C (1993) Inorg Chem 32:4139
33. Mallet C, Thummel RP, Hery C (1993) Inorg Chim Acta 210:223
34. Piguet C, Bunzli J-CG, Bernardinelli G, Bochet CG, Froidevaux P (1995) J Chem Soc Dalton Trans 83
35. Bardwell DA, Jeffery JC, Jones PL, McCleverty JA, Psillakis E, Reeves Z, Ward MD (1997) J Chem Soc Dalton Trans 2079
36. Semenova LI, Sobolev AN, Skelton BW, White AH (1999) Aust J Chem 52:519
37. Li Y, Huffman JC, Flood AH (2007) Chem Commun 2692
38. Meudtner RM, Ostermeier M, Goddard R, Limberg C, Hecht S (2007) Chem Eur J 13:9834
39. Bettencourt-Dias Ad, Barber PS, Viswanathan S, de Lill DT, Rollett A, Ling G, Altun S (2010) Inorg Chem 49:8848
40. Yip Y-W, Wen H, Wong W-T, Tanner PA, Wong K-L (2012) Inorg Chem 51:7013
41. Andreiadis ES, Imbert D, Pecaut J, Demadrille R, Mazzanti M (2012) Dalton Trans 41:1268
42. Shavaleev NM, Eliseeva SV, Scopelliti R, Bunzli J-CG (2014) Inorg Chem 53:5171
43. Hargittai M, Hargittai I (1992) Int J Quantum Chem 44:1057
44. Cordero B, Gómez V, Platero-Prats AE, Revés M, Echeverría J, Cremades E, Barragán F, Alvarez S (2008) Dalton Trans 2832
45. Shannon RD, Prewitt CT (1970) Acta Cryst B26:1046
46. Zheng J, Alecu IM, Lynch BJ, Zhao Y, Truhlar DG. Unpublished results by I. M. Alecu. http://comp.chem.umn.edu/freqscale/version3b2.htm. Last accessed 04 July 2015
47. Dennington R, Keith T, Millam J (2009) GaussView, version 5. Semichem Inc., Shawnee Mission
48. Paul P, Ghosh M, Neogy D, Mallick PK (2011) Spectrochim Acta A 78:59